Geomechanics and Engineering, *Vol. 23, No. 2 (2020) 151-163*
DOI: https://doi.org/10.12989/gae.2020.23.2.151

Grouting diffusion mechanism in an oblique crack in rock masses considering temporal and spatial variation of viscosity of fast-curing grouts

Shuling Huang[1], Qitao Pei*[1,2], Xiuli Ding[1], Yuting Zhang[1], Dengxue Liu[1], Jun He[1] and Kang Bian[3]

[1]Key Laboratory of Geotechnical Mechanics and Engineering of Ministry of Water Resources, Changjiang River Scientific Research Institute, Wuhan, Hubei 430010, China
[2]Wuhan Municipal Engineering Design & Research Institute Co., Ltd., Wuhan 430023, China
[3]State Key Laboratory of Geomechanics and Geotechnical Engineering, Institute of Rock and Soil Mechanics, Chinese Academy of Sciences, Wuhan, Hubei 430071, China

(Received March 23, 2020, Revised July 21, 2020, Accepted September 28, 2020)

Abstract. Grouting method is an effective way of reinforcing cracked rock masses and plugging water gushing. Current grouting diffusion models are generally developed for horizontal cracks, which is contradictory to the fact that the crack generally occurs in rock masses with irregular spatial distribution characteristics in real underground environments. To solve this problem, this study selected a cement-sodium silicate slurry (C-S slurry) generally used in engineering as a fast-curing grouting material and regarded the C-S slurry as a Bingham fluid with time-varying viscosity for analysis. Based on the theory of fluid mechanics, and by simultaneously considering the deadweight of slurry and characteristics of non-uniform spatial distribution of viscosity of fast-curing grouts, a theoretical model of slurry diffusion in an oblique crack in rock masses at constant grouting rate was established. Moreover, the viscosity and pressure distribution equations in the slurry diffusion zone were deduced, thus quantifying the relationship between grouting pressure, grouting time, and slurry diffusion distance. On this basis, by using a 3-d finite element program in multi-field coupled software Comsol, the numerical simulation results were compared with theoretical calculation values, further verifying the effectiveness of the theoretical model. In addition, through the analysis of two engineering case studies, the theoretical calculations and measured slurry diffusion radius were compared, to evaluate the application effects of the model in engineering practice. Finally, by using the established theoretical model, the influence of cracking in rock masses on the diffusion characteristics of slurry was analysed. The results demonstrate that the inclination angle of the crack in rock masses and azimuth angle of slurry diffusion affect slurry diffusion characteristics. More attention should be paid to the actual grouting process. The results can provide references for determining grouting parameters of fast-curing grouts in engineering practice.

Keywords: fast-curing grout; oblique crack; grouting; multi-field coupling; diffusion mechanism

1. Introduction

A grouting method is an important way to strengthen weak and unfavorable geological bodies, improve overall stability and strength of surrounding rocks, and block the flow of groundwater, so it has been rapidly developed for use in disaster management applications in underground engineering (Lisa *et al.* 2012, Seo *et al.* 2016, Cheng *et al.* 2019). However, the grouted slurry will encounter complex hydraulic conditions in the treatment of high pressure and large flow water inrush disasters, in which dynamic hydraulic pressure easily scours and dilutes traditional single cement liquid, causing failure in stopping up water and rock mass reinforcement. Therefore, the anti-washout property and gelling performance of slurry are crucial for the success of grouting in the treatment of water inrush disasters.

Fast-curing grout is a kind of grouting material that can solidify quickly. It is generally composed of grouting material and gelling material. Two independent grouting systems are used. The materials are mixed before grouting or inside the grouting hole, and afterwards grouted into cracks. Compared to chemical grouting, fast-curing grouting is environmentally friendly, low-cost, and able to achieve satisfactory impermeability and excellent durability (Mirza *et al*. 2013, Celik and Canakci 2015, Devi *et al*. 2019). As generally used fast-curing grouting materials, cement-sodium silicate slurry (C-S slurry) are widely applied in grouting engineering of rock masses due to advantages, such as fast-curing, high early strength, high retention rate, and controllable setting time (Bezuijen *et al.* 2011, Zhang *et al.* 2017, Zhou *et al.* 2019, Zhou *et al.* 2020). In recent years, according to different conditions of the rock-soil media encountered during grouting, many new types of grouting materials and equipment have been developed and put into use, to such an effect that helps to strengthen weak rocks; however, grouting theory develops slowly, so that the grouting parameters are designed relatively blindly and with uncertainty. Therefore, it is important to investigate grout diffusion theory.

At present, scholars have carried out much research into

*Corresponding author, Associate Professor, Ph.D.
E-mail: peiqitao@126.com

http://www.techno-press.org/?journal=gae&subpage=7

ISSN: 2005-307X (Print), 2092-6219 (Online)

the diffusion and migration characteristics of slurry in rock-soil media from different perspectives. In accordance with different constitutive equations of grouting theory, the type of slurry can be treated as a Newtonian fluid (Fransson *et al.* 2007), Bingham fluid (Dahlo and Nilsen 1994, Yoon and Mohtar 2015), power law fluid (Bouchelaghem 2009), etc. Based on the equations of motion of the slurry, the slurry diffusion mode includes permeation grouting (Funehag and Gustafson 2008), compaction grouting (Miller and Roycrof 2004), fracture grouting (Groutenhuis 2004), and grouting with flowing water (Ruan 2005). Fast-curing binary grouts widely used in grouting processes have characteristics, such as a short curing time and highly time- and space-varying diffusion characteristics. In view of these characteristics, Ruan (2005) established a grouting diffusion model for cracked rock masses considering time variation of viscosity of slurry through laboratory testing and theoretical analysis. Based on capillary penetration theory, Sha *et al*. (2013) conducted a systematical research on the effects of different components and proportions of the slurry on the mechanical properties of consolidation body, the liquidity and permeability of slurry. By considering time variation and non-uniform spatial distribution of viscosity of slurry, Zhang *et al*. (2015) established a diffusion model of slurry in horizontal cracks which considered temporal and spatial variations in the viscosity of slurry. Celik (2019) compared the permeation grouting method to reinforce soil using different grout flow models. Meanwhile, many numerical simulation methods, such as the FEM/VOF method (Chen *et al.* 2014) and step-by-step calculation methods (Kim *et al.* 2009, Zhang *et al.* 2017) have been used to simulate diffusion processes in slurry to good effect. Furthermore, based on engineering practice, some scholars have studied strengthening effects of grouting by real-time, in situ monitoring (Andjelkovic *et al.* 2013, Zhong *et al.* 2015, Zhou *et al*. 2020).

In general, a majority of the current theories assume a horizontal orientation for cracks and then cannot take into account the dead weight of slurry in cracks with an oblique orientation. If a slurry diffusion theory based on horizontally oriented crack assumption is adopted to predict the fast-setting grouting process of an obliquely oriented crack, then the calculated grouting pressure would considerably deviates from the actual situation, thus restricting the application effect of grouting technology.

To address the above issue, this paper selects the commonly used C-S slurry as grouting material. The viscosity time-varying Bingham fluid constitutive model and fluid mechanics theory are adopted considering the effect of slurry dead weight. The grout diffusion process for quick-setting slurry in cracks with arbitrary orientations is studied and a theoretical model for slurry diffusion in cracks with oblique orientations is proposed to reflect the spatio-temporal variation of slurry viscosity. Then, the relationship linking grouting pressure, grouting time, and slurry diffusion distance is determined. By employing a 3-d finite element program in the multi-field coupled software Comsol, the diffusion process of fast-curing grouts in the crack was simulated, further verifying feasibility of the theoretical model. In addition, by analysing measured grouting data in the field in two actual engineering projects, the application effects of the model in engineering was further evaluated. On this basis, the influence of crack occurrence in rock masses on diffusion characteristics of slurry is further discussed. The results can provide references for engineering application of C-S slurry.

2. Slurry diffusion model in an oblique crack in a rock mass

2.1 Diffusion process and basic assumptions of fast-curing grout behaviour

The existing research demonstrates that fast-curing grouts require little time for gelation, ranging from a few tens of seconds to a few minutes. If the single-fluid grouting method is used, grouting pipelines are easily blocked, so the double-liquid mixing method is used for grouting the vast majority of fast-curing grouts (such as C-S slurry). As shown in Fig. 1, in the grouting process in a cracked rock mass, slurries A and B were transported via independent grouting pipes and mixed before or after entering grouting holes and then grouted into cracks. After mixing, a physico-chemical reaction occurred between them and the viscosity began to increase.

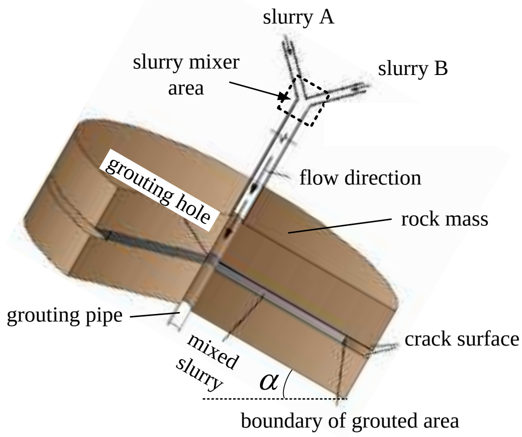

(a) General sketch

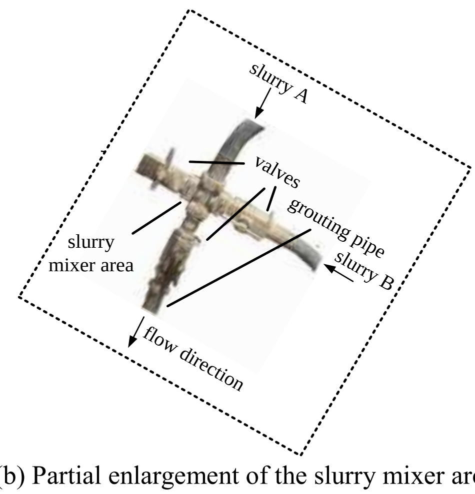

(b) Partial enlargement of the slurry mixer area

Fig. 1 Diagram of oblique crack grouting of fast-curing grouts

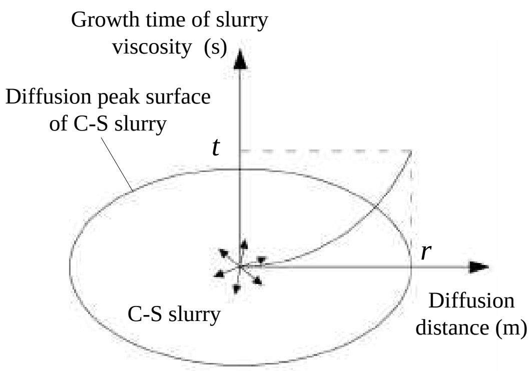

Fig. 2 Variation of C-S slurry viscosity with time and space

Table 1 List of symbols used in equations

Symbol	Description	Symbol	Description	Symbol	Description
α	Inclination angle of the crack	b	Aperture of the crack	r	Flow direction of slurry
θ	Azimuth angle of slurry diffusion	z	Spatial distance	ρ	Fluid density
A , B	Viscosity constants of slurry determined by injection tests	F_r	Weight component of fluid per unit mass along the r-direction	$\mu_p(t)$	Time function of viscosity of slurry
r_t	Diffusion distance of slurry at moment t	τ	Shear stress of slurry	τ_0	Yield shear stress of slurry
u	Fluid velocity vector	u_r	Velocity component along the r-axes	u_θ	Velocity component along the θ-axes
$\bar{u}$	Average velocity of slurry in the crack	$-du/dz$	Shear rate of slurry	μ	Viscosity of slurry
μ_g	Viscosity of grouting	μ_w	Viscosity of water	T	Time
p	Fluid pressure	s_g	Volume fraction of slurry	s_w	Volume fraction of water
F	Force per unit volume	I	3-order unit matrix	∇	Hamiltonian operator

As demonstrated in Fig. 2, in the slurry diffusion zone, the time for transporting slurry in the grouting holes was the shortest and viscosity was the lowest, while the diffusion peak surface of the slurry showed the longest diffusion time and the highest viscosity. The spatial distribution of viscosity was non-uniform.

In the actual grouting process, a grouting section generally has several cracks requiring grouting. For this reason, and to facilitate the study, this research only considered the situation of grouting into a single crack. This is the basis for analyzing slurry diffusion in grids with multiple cracks.

According to the diffusion characteristics of fast-curing grouts in the grouting process, the assumptions of the calculation model are listed as follows:

(1) Slurry and water are regarded as homogeneous, isotropic, incompressible fluids (Frank 2015).

(2) Except for that in the surrounds of the grouting holes, slurry flow is considered as streamline flow and the ratio and flow pattern of slurry are unchanged in the grouting process.

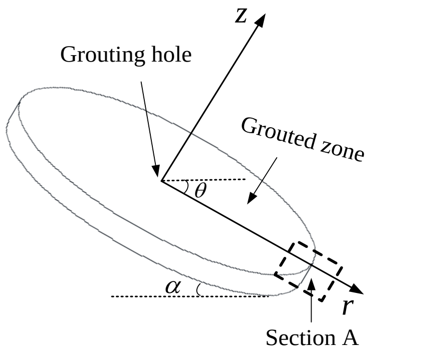

(a) Position of infinitesimal slurry element

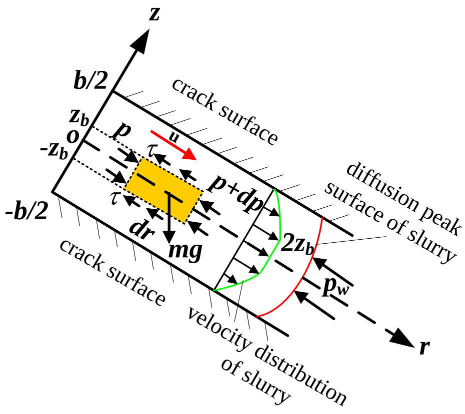

(b) Force analysis for section A

Fig. 3 Schematic map of the force of the slurry flow

(3) Suppose there is no slip on the rigid wall boundary, that is, the slurry will not flow into rock masses through the crack wall in the flow process (John 1995).

(4) Slurry diffuses in the mode of complete displacement and the dilution effects of water in the interface of slurry and water phases on viscosity of slurry are ignored.

(5) Slurry only diffuses in the cracks in a rock mass, without considering grout loss caused by infiltration of slurry into rock masses on both sides of the crack.

2.2 Equation of motion for slurry diffusion

To facilitate the description, Table 1 defines all symbols that are used to express the various equations hereinafter.

Owing to fast-curing grouts having time-varying viscosity, the equation of a Bingham fluid is used to describe the constitutive equations of this slurry:

$$\tau = \tau_0 + \mu_P(t) \cdot \left(-\frac{du}{dz}\right) \tag{1}$$

where, τ, τ_0, $\mu_p(t)$, $-du/dz$, u, and z indicate the shear stress of slurry, the yield shear stress of slurry, the time function of viscosity of slurry, the shear rate of slurry, the flow velocity of slurry, and the spatial distance, respectively.

It is assumed that fast-curing binary grouts flowed radially in a crack comprising two flat, smooth plates. It is supposed that b and α represent the aperture and the inclination angle of the crack, r denotes the flow direction of slurry and the origin of coordinates on the r-axis is on the axis of the grouting hole. In addition, z refers to the aperture direction of the crack and the origin of coordinates of the z-axis is located in the centre of the crack. Moreover, θ indicates the angle between the tendency line of the crack surface and the flow direction of slurry (referred to as the azimuth angle of slurry diffusion). The schematic diagram of slurry diffusion on the oblique crack surface in the cylindrical coordinate system (r, θ, z) was established (Fig. 3(a)). Plane A, perpendicular to the crack through the grouting hole, was selected for study. By taking the centre of the crack as the axis of symmetry, the micro-body of the slurry was selected for stress analysis (Fig. 3(b)). In the figure, slurry was in the space formed by the top and bottom surfaces of the crack and hydrostatic pressure were applied to the slurry surface.

For incompressible viscous fluid, the continuity equation of motion is written as:

$$\frac{\partial u_r}{\partial r}+\frac{1}{r}\frac{\partial u_\theta}{\partial \theta}+\frac{\partial u_z}{\partial z}+\frac{u_r}{r}=0 \tag{2}$$

Slurry moved along the r-axis and the flow velocity in the z-direction is zero, so $u_z = 0$ and $u_\theta = 0$, thus obtaining:

$$\frac{\partial u_r}{\partial r}=-\frac{u_r}{r} \tag{3}$$

A microhexahedron of fluid was selected for stress analysis. Based on Newton's laws of motion, the momentum equation of the motion of a viscous fluid in an inertial system is obtained. The inertial frame hereinafter can be defined as a reference frame as follows: when the object is not under force, it will maintain a relatively still or uniform linear motion state. The time is uniformly elapsed and the space is uniform and isotropic.

The equation along the r-axis in the cylindrical coordinate system is shown as follows:

$$\rho\left(\frac{du_r}{dt}-\frac{u_\theta^2}{r}\right)=\rho F_r+\frac{1}{r}\left[\frac{\partial(rp_{rr})}{\partial r}+\frac{\partial p_{r\theta}}{\partial \theta}+\frac{\partial(rp_{zr})}{\partial z}\right]-\frac{p_{\theta\theta}}{r} \tag{4}$$

where, ρ represents the fluid density; u_r and u_θ indicate the velocity components along the r- and θ-axes; F_r denotes the weight component of fluid per unit mass in the r-direction. p_{rr}, $p_{r\theta}$, p_{zr} and $p_{\theta\theta}$ are pressure per unit area. They can be expressed by p_{ij} as: term p_{ij} is the stress vector on the unit area. The first subscript indicates the outer normal direction of the stress action surface, and the second subscript denotes the direction of the stress component.

In accordance with Eq. (1), the stress-flow velocity relationship is determined.

$$\begin{cases} p_{rr}=-(p-\tau_0)+2\mu_p(t)\cdot\dfrac{\partial u}{\partial r} \\ p_{\theta\theta}=-(p-\tau_0)+2\mu_p(t)\cdot\left(\dfrac{1}{r}\dfrac{\partial u_\theta}{\partial \theta}+\dfrac{u}{r}\right)=-(p-\tau_0)-2\mu_p(t)\cdot\dfrac{\partial u}{\partial r} \\ p_{zz}=-(p-\tau_0)+2\mu_p(t)\cdot\dfrac{\partial u_z}{\partial z}=-(p-\tau_0) \\ p_{\theta r}=\mu_p(t)\cdot\left(\dfrac{1}{r}\dfrac{\partial u_r}{\partial \theta}+\dfrac{\partial u_\theta}{\partial r}-\dfrac{u_\theta}{r}\right)+\tau_0=\dfrac{\mu_p(t)}{r}\dfrac{\partial u_r}{\partial \theta}+\tau_0 \\ p_{zr}=\mu_p(t)\cdot\left(\dfrac{\partial u_z}{\partial r}+\dfrac{\partial u_r}{\partial z}\right)+\tau_0=\mu_p(t)\cdot\dfrac{\partial u_r}{\partial z}+\tau_0 \end{cases} \tag{5}$$

By substituting Eqs. (2)-(4) into Eq. (3), high-order terms are neglected. Moreover, p_{zr} and u_r are recorded as τ and u, so we have:

$$\frac{d\tau}{dz}=\frac{dp}{dr}-\rho g\sin\alpha\, g\cos\theta \tag{6}$$

Based on analysis of the differential equation governing the force balance on the unit, the equations of shear stress and velocity distribution on the cross-section are obtained:

$$\tau=\begin{cases} 0 & (-z_b<z<z_b) \\ \tau_0 & (z=\pm z_b) \\ \dfrac{\tau_0 b}{2z_b} & (z=\pm\dfrac{b}{2}) \\ \dfrac{z}{z_b}\tau_0 & (z_b\le|z|\le\dfrac{b}{2}) \end{cases} \tag{7}$$

A flow plug is present in the flow of a Bingham fluid, so the height of flow plug changes with pressure gradient during slurry flow. Due to the large fluid resistance, the diffusion range of C-S slurry under certain grouting pressures is much smaller than that of cement slurry. Therefore, the changes in the height of the flow plug cannot be ignored and the height of the flow plug is $2z_b$.

Let $p^*=p-\rho gr\sin\alpha\cdot\cos\theta$, by substituting this into Eq. (6) for integral operation, $\tau=z\mathrm{d}p^*/\mathrm{d}r$ is obtained and substituted into Eq. (1) to obtain:

$$\frac{du}{dz}=\frac{z_b-z}{\mu_p}\cdot\frac{dp^*}{dr} \tag{8}$$

The above equation is integrated, thus obtaining

$$u=\begin{cases} -\dfrac{1}{2\mu_p}\cdot\dfrac{dp^*}{dr}\left(\dfrac{b}{2}-z_b\right)^2 & (-z_b<z<z_b) \\ -\dfrac{1}{2\mu_p}\cdot\dfrac{dp^*}{dr}\left[\left(\dfrac{b}{2}\right)^2-z^2-2z_b\cdot\left(\dfrac{b}{2}-z\right)\right] & (z_b\le|z|\le\dfrac{b}{2}) \end{cases} \tag{9}$$

The average velocity $\bar{u}$ of slurry in the crack is:

$$\bar{u}=\frac{1}{b}\int_{-\frac{b}{2}}^{\frac{b}{2}}u\,dz=-\frac{b^2}{12\mu_p}\left(\frac{dp^*}{dr}-\frac{3\tau_0}{b}+\frac{4\tau_0^3}{b^3}\cdot\left(\frac{dp^*}{dr}\right)^{-2}\right) \tag{10}$$

The second-order term $-\frac{\tau_0{}^3}{3b\mu_p}\cdot(\frac{dp^*}{dr})^{-2}$ is ignored, thus obtaining

$$\bar{u}=-\frac{b^2}{12\mu_p}\left(\frac{dp^*}{dr}-\frac{3\tau_0}{b}\right) \tag{11}$$

2.3 Spatial and temporal distribution of pressure in slurry diffusion zone

Firstly, the geometrical morphology of diffusion of slurry on the crack surface was analyzed. Supposing that the increase in viscosity of the slurry is bounded, when the motion velocity of slurry is $\bar{u}=0$, the slurry stops flowing and Eq. (10) can be changed to:

$$\left(\frac{dp^*}{dr}+\frac{\tau_0}{b}\right)\left(\frac{dp^*}{dr}-2\frac{\tau_0}{b}\right)^2=0 \tag{12}$$

Owing to pressure gradient dp/dr reducing along the r-axis:

$$\frac{dp^*}{dr} = -\frac{\tau_0}{b} \tag{13}$$

By substituting $p^* = p - \rho g r \sin\alpha \cdot \cos\theta$ into the above equation and integrating to r_{max} from radius r_0, we get

$$r_{max} - r_0 = \frac{\Delta p \cdot b}{\tau_0 - \rho g b \sin\alpha \cdot \cos\theta} = \frac{\varepsilon_p}{1 - e \cdot \cos\theta} \tag{14}$$

where $e = \frac{\rho g b \sin\alpha}{\tau_0}$ and $\varepsilon_p = \frac{(p_0 - p_w)^b}{\tau_0}$.

In accordance with Eq. (14), the diffusion trajectory of slurry appeared as an ellipse. Without considering the influences of viscosity of slurry, the eccentricity e mainly depends on the density of the slurry, yield shear stress, inclination angle of crack surface, and equivalent hydraulic aperture.

The present studies (Wang and Su 2002, Groutenhuis 2004) show that the equivalent hydraulic aperture of single cracks is smaller than the average aperture (or mechanical aperture). When other micro-cracks in rock masses are ignored, the value is generally at millimetre-level. Furthermore, the yield shear stress τ_0 of a single-fluid cement slurry is generally a few pascals, while that of C-S slurry is much larger. The eccentricity e of an ellipse is usually less than 0.1 and close to that of a circle. Therefore, for fast-curing grouts whose viscosity increases rapidly with time, and of which the diffusion range is not large, for convenience of analysis, it is considered that the geometrical morphology of diffusion trajectory of slurry is approximately circular under hydrostatic pressure. Theoretical analysis and numerical simulation both demonstrate that the error resulting from such an approximate treatment is acceptable and can meet engineering requirements.

In the flow of slurry, the following equations are obtained according to the law of conservation of mass:

$$\bar{u} = \frac{q}{2\pi \mathrm{rb}} = -\frac{b^2}{12\mu_p}\left(\frac{dp^*}{dr} - \frac{3\tau_0}{b}\right) \tag{15}$$

$$\frac{dp^*}{dr} = -\frac{6\mu_p q}{\pi r b^3} + \frac{3\tau_0}{b} \tag{16}$$

At moment t, diffusion distance r_t is:

$$r_t = \sqrt{\frac{qt}{2\pi b}} \tag{17}$$

By putting $p^* = p - \rho g r \sin\alpha \cdot \cos\theta$ into Eq. (16), we have:

$$\frac{dp}{dr} = -\frac{6\mu_p q}{\pi r b^3} + \frac{3\tau_0}{b} + \rho g \sin\alpha\, g \cos\theta \tag{18}$$

The positions of slurry from r to that at time t are integrated, thus obtaining

$$p(r,t) = \frac{6q}{\pi b^3}\int_r^{\sqrt{\frac{qt}{2\pi b}}} \frac{\mu_p}{r} dr - \left(\frac{3\tau_0}{b} + \rho g \sin\alpha \cdot \cos\theta\right) \cdot \left(\sqrt{\frac{qt}{2\pi b}} - r\right) + P_w \tag{19}$$

Based on the viscosity-time characteristics of fast-curing grouts, the simplified viscosity-time function is used for fitting, that is:

$$\mu(t) = At^B \tag{20}$$

where, A and B are constants.

By substituting Eq. (20) into Eq. (19), the equation governing the spatio-temporal distribution of grouting pressure, namely the p-r-t relationship, is:

$$p(r,t) = \frac{3qA}{\pi B b^3}\left[t^B - \left(\frac{2\pi b r^2}{q}\right)^B\right] - \left(\frac{3\tau_0}{b} + \rho g \sin\alpha\, g\cos\theta\right)\left(\sqrt{\frac{qt}{2\pi b}} - r\right) + p_w \tag{21}$$

The grouting pressure-time distribution relationship, that is, the p-t relationship is expressed as:

$$p(t) = \frac{3qA}{\pi B b^3}\left[t^B - \left(\frac{2\pi b r_0^2}{q}\right)^B\right] - \left(\frac{3\tau_0}{b} + \rho g \sin\alpha\, g\cos\theta\right)\left(\sqrt{\frac{qt}{2\pi b}} - r_o\right) + p_w \tag{22}$$

The grouting pressure-space distribution relationship, that is, the p-r relationship is:

$$p(r) = \frac{3qA}{\pi B b^3}\left(\frac{2\pi b}{q}\right)^B [r^{2B} - r_0^{2B}] - \left(\frac{3\tau_0}{b} + \rho g \sin\alpha\, g\cos\theta\right)(r - r_0) + p_w \tag{23}$$

When the inclination angle α of the crack surface in rock masses is zero, that is, cracks are formed by horizontal planes, the reduced Eqs. (21)-(23) are consistent with the derivation results published elsewhere (Zhang *et al.* 2015). This indicates that the theoretical model of slurry diffusion established in the paper has generality and the diffusion model in cracks on horizontal planes is just a special case thereof. The research also shows that, when fast-curing grouts diffuse along an oblique crack, grouting pressure is mainly determined by four factors: the viscosity of the slurry, yield shear stress, occurrence of the crack, and hydrostatic pressure.

3. Validation of effectiveness of the theoretical model

To verify the feasibility of the theoretical model of grouting, in this section, a 3-d finite element analysis model was built based on multi-field coupled software Comsol. This section simulated the diffusion process of fast-curing grouts in the crack and compared the numerical simulation results with theoretical calculation values. In addition, by analysing the measured grouting data from two engineering case studies, and comparing them with theoretical calculation values, the efficacy of the model in engineering practice was evaluated.

3.1 Numerical simulation analysis

3.1.1 Model construction and calculation conditions

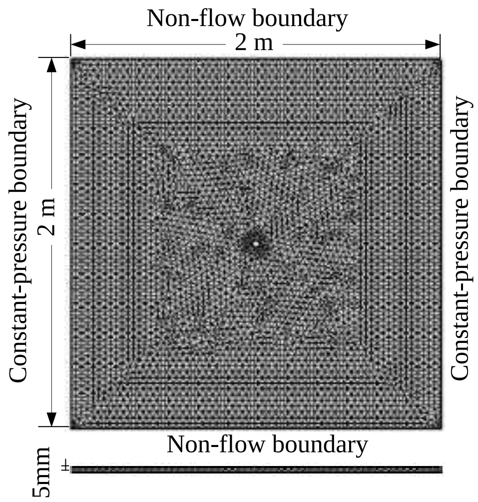

Fig. 4 Mesh generation and boundary conditions

Table 2 Calculation parameters for grouting in an oblique crack

Crack aperture in rock mass /b (mm)	Radius of grouting hole /r0 (mm)	Grouting flow rate /q (L/min)	Grouting time /t (s)	Pressure at boundary of grouted zone /Pw (kPa)
5	0.02	15	60	0.2

The 3-d finite element analysis model measured 2 m × 2 m × 0.005 m and the grouting hole was in the geometrical centre of the model. The left and right boundaries of the model were set to be constant-pressure boundaries with hydrostatic pressure, from which the slurry and water that entered the crack flowed. The upper and lower boundaries, and boundaries on both sides of the model, were non-flow boundaries and met the non-slip boundary condition. At the initial moment, the model was filled with water, while after grouting, slurry entered the crack space from the grouting hole at a constant rate. The free triangular grids were used in the model and grids close to the grouting hole were properly densified. The grid division and boundary conditions of the finite element model are shown in Fig. 4 and parameters for grouting in the crack are listed in Table 2.

3.1.2 Parameters of fast-curing binary grouts and fluid control equation

In this research, the fast-curing materials were C-S slurry. The slurry contained 42.5 R ordinary silicate cement and its property conformed to the standard specified in Common portland cement (GB175-2007)31. Conventional sodium silicate was used and its modulus, Baume degree, and density were 3.0, 40 Be, and 1.38 g/cm^3, respectively. The C-S slurry included two compositions, i.e., cement and sodium silicate. Of them, the water cement ratio in the cement was 1:1 and the volume ratio of cement to sodium silicate was C:S = 1:1. In the first 70 s of the reaction at 20°C, when the water cement ratio of cement slurry was C:W = 1:1 and the volume ratio of cement to sodium silicate was C:S = 1:1, the apparent viscosity–time relationship of C-S slurry, provided by Li *et al*. (2013), is shown as follows:

$$\mu(t) = 0.003182 \times t^{2.23} \tag{24}$$

By solving Eqs. (17)-(24) simultaneously, the spatial distribution function of viscosity of slurry is shown in Eq. (25) and its spatial distribution characteristics are demonstrated in Fig. 5.

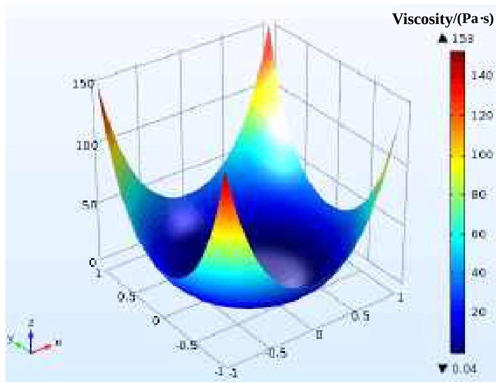

Fig. 5 Spatial distribution curves of viscosity of the slurry

$$\mu(r,t) = 0.003182 \times \left[\frac{2\pi b(x^2+y^2)}{q}\right]^{2.23} \tag{25}$$

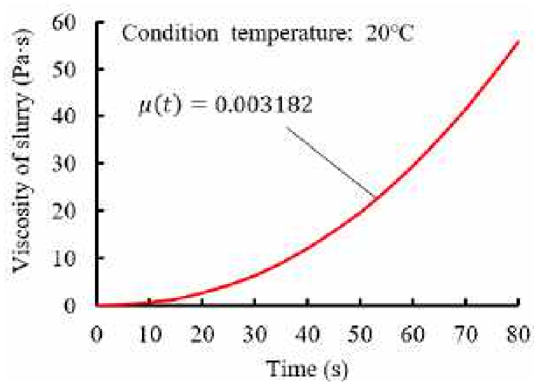

(a) Curve of slurry viscosity versus time

(b) SV-100 vibrating type viscometer

Fig. 6 Viscosity curve of C-S slurry and viscometer (Li *et al*. 2013)

The relationship between chemical reaction time and viscosity of C-S slurry is displayed in Fig. 6(a). The viscosity of slurry was determined by using the SV-100 vibrating string viscosimeter (Fig. 6(b)) produced by AND Co., Japan, and could continuously record measurement data.

In the slurry mixing zone, the viscosity of the mixed fluid is defined as the average viscosity after mixing slurry with water and is calculated as follows:

$$\begin{cases} \dfrac{1}{\mu} = S_g \dfrac{1}{\mu_g} + S_w \dfrac{1}{\mu_w} \\ S_g + \ S_w = 1 \end{cases} \tag{26}$$

where, s_{g} and s_{w} represent the volume fractions of slurry and water; μ_{g}, μ_{w}, and μ indicate the viscosities of slurry, water, and their mixture, respectively.

The Navier-Stokes equation is used to represent motion of the fluid. Under 3-d conditions, the constitutive relationship between fluid motion and stress is:

$$\rho \frac{\partial u}{\partial t} + \ \rho(\mu\nabla)u = \nabla[-pI + \mu(t)(\nabla u + (\nabla u)^T)] + F \tag{27}$$

where, ρ, p, t, u, $\mu(\mathrm{t})$, F, I, and $\bigtriangledown$ represent the fluid density, fluid pressure, time, fluid velocity vector, the function of fluid viscosity, the force per unit volume, the 3-order unit matrix, and the Hamiltonian operator, respectively.

Ignoring the compressibility of slurry and water, the densities of slurry and water are considered as constants. By analysing characteristic units in the crack space, based on the law of conservation of mass, mass differences of the slurry and water flowing into, and out of, the unit separately equal mass changes in the amount of slurry and water in the unit, thus obtaining the following continuity equations:

$$\begin{cases} -\nabla(S_{\mathrm{g}} \cdot u) = \dfrac{\partial(S_{\mathrm{g}})}{\partial t} \\ -\nabla(S_w \cdot u) = \dfrac{\partial(S_w)}{\partial t} \end{cases} \tag{28}$$

3.1.3 Comparisons between theoretical calculation and numerical simulation results

In the numerical analysis, by setting inclination angle a to be 0° and 30°, and the azimuth angle θ of the crack to be 0° and 180°, the slurry diffusion process and pressure distribution characteristics during grouting in the oblique crack were simulated. The comparisons between calculated and simulated values of grouting pressure in different crack occurrences are presented in Fig. 7. At t = 35 s and 55 s, the comparisons between calculated and simulated values of grouting pressure in slurry diffusion zone are as shown in Fig. 8. The following conclusions can be obtained:

(1) The trends in the grouting pressure-time and grouting pressure-space curves obtained through theoretical calculation and numerical simulation are consistent. The difference between them is small and the maximum error is no more than 10%, which indicates that the theoretical calculation values obtained in this study matched the numerical simulation results, further verifying the effectiveness of the theoretical model.

(2) Theoretical values of grouting pressure are slightly larger than the numerical simulation results. This is caused by the inconsistency between theoretical analysis and numerical simulation methods. In the theoretical analysis, it is assumed that the slurry diffusion method is complete

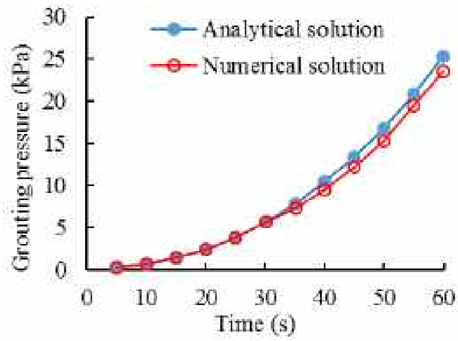

(a) Inclination angle, 0°

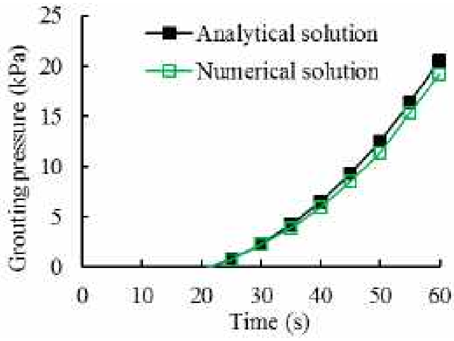

(b) Inclination angle, 30° and Azimuth, 0°

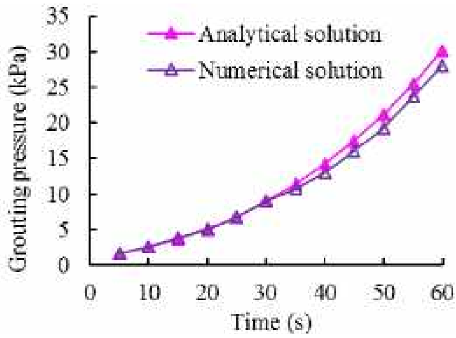

(c) Inclination angle, 30° and Azimuth, 180°

Fig. 7 Curves of grouting pressure versus time

displacement diffusion, and the dilution effect of water on the slurry-water interface is not considered. In the numerical simulation process, the dilution effect of water on the slurry is considered. The viscosity of the fluid is lower than the viscosity of the slurry, thus resulting in the viscosity resistance of the slurry diffusion in the numerical simulation being lower than the theoretical value. Therefore, the theoretically calculated grouting pressure is higher than the simulated value.

(3) Grouting pressure shows exponential growth with time. In the early stage of grouting, the rate of growth of the grouting pressure is small, while it increases in its later stages, which is consistent with the exponential function relating the viscosity of the slurry and time in Eq. (24).

(4) From the grouting hole to the surrounding, the grouting pressure is attenuated. With increasing distance from the grouting hole, the rate of attenuation of grouting pressure gradually increases. In the early stages of grouting, the viscosity of the slurry is low and the grouting pressure attenuates slowly. In the later stages, the viscosity of the slurry near the diffusion front is much higher than that near

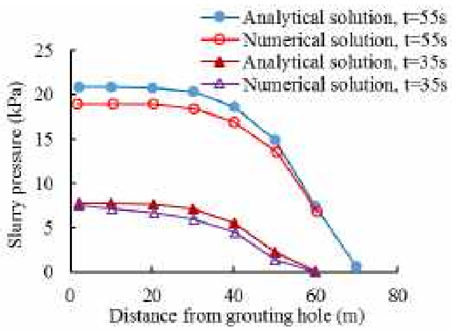

(a) Inclination angle, 0°

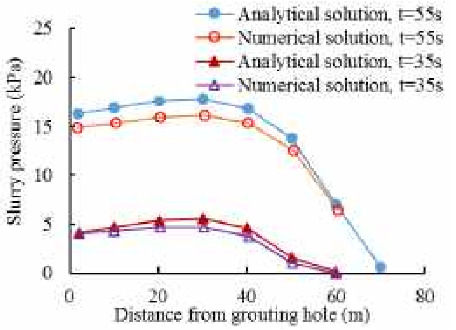

(b) Inclination angle, 30° and Azimuth, 0°

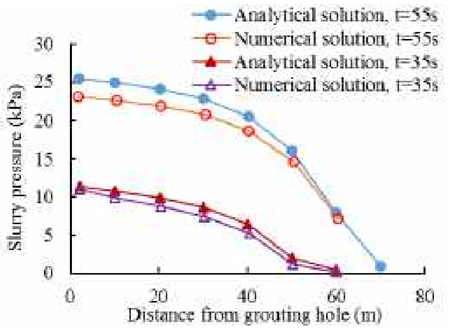

(c) Inclination angle, 30° and Azimuth, 180°

Fig. 8 Spatial distribution of slurry pressure at different time

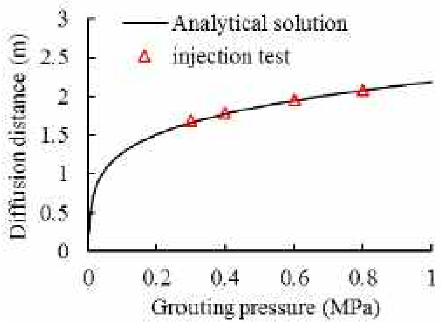

(a) Fault f_1

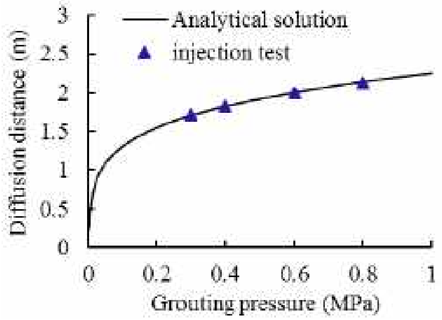

(b) Fault f_2

Fig. 9 Curves of grouting pressure near the faults versus diffusion distance

the grouting hole, resulting in the pressure gradient in the diffusion peak surface of the slurry being far greater than that around the grouting hole. Therefore, the grouting pressure decreases rapidly and shows non-linear characteristics.

In conclusion, the results obtained using the theoretical model established in the study and the numerical analysis favourably represent slurry diffusion processes in fast-curing grouts along an oblique crack. By utilising the proposed model, the design parameters for grouting, such as final grouting pressure, grouting rate, and diffusion radius of slurry, can be estimated.

3.2 Case study analysis

3.2.1 Case 1: Grouting engineering of Shahe reservoir, Jilin Province, China

Shahe reservoir, built in 1958, is located in Shulan City (Ruan 2005), Jilin Province, China. In 1985, the reservoir was expanded to its current size and suffers from seepage around the mountain on the dam shoulder, overflow, and dispersive seepage behind the dam. Cracks have developed in surrounding rock masses. Fault f_1 trends to 104° with an inclination angle of 61°, while fault f_2 shows a strike of 112° and an inclination angle of 63°. The cracks are open cracks and their widths were determined through analysis of a water pump-in test. The equivalent hydraulic width was about 2.0 mm, and the grouting rate and the diameter of grouting hole were 90 L/min and 59 mm, respectively. The lengths of grouted sections were 2.0, 2.5, 3.8, and 4.2 m and the corresponding grouting pressures were 0.3 MPa, 0.4 MPa, 0.6 MPa, and 0.8 MPa. Fig. 9 shows the relationship between grouting pressure near the fault zone and the slurry diffusion radius obtained using the proposed model. Table 2 lists the comparisons of calculation results obtained by utilising the model, the Lombardi formula (Lombardi 1989), and the Wittke formula (Wittke 1991) with slurry diffusion radii measured in the field under the given grouting pressure.

3.2.2 Case 2: Grouting the dam foundation, Shanggou Hydropower Station

Shanggou Hydropower Station is located in Dunhua City, Jilin Province, China and belongs to a cascade hydropower station scheme on the main stream of the Mudanjiang River (Ruan 2005). Structural planes of cracks mainly showed primary joint fissures and the crack widths were determined by analysis of data from a water pump-in test. Moreover, the average inclination angle of the cracks was 86°. The five-spot and single-spot methods were used for the water pump-in test. In the test, the single-spot pressure water test refers to the pressure water with a single pressure magnitude of 1.0 MPa. The water injecting duration is 20 minutes and the permeability is calculated based on the final value. The five-spot method contains five processes with varying magnitudes of water loads, such as

Table 3 Comparison of theoretical diffusion radius with measured data, dam foundation, Shahe Reservoir

Faults	Theoretical diffusion radius (m)	Measured diffusion radius (m)	Calculated diffusion radius by Lombardi and Wittke (m)
f_1	1.69 ~ 2.08	1.5 ~ 2.0	11.1 ~ 43.7
f_2	1.72 ~ 2.13	1.5 ~ 2.0	11.1 ~ 43.7

Table 4 Comparison of theoretical diffusion radius with measured data, dam foundation, Shanggou Hydropower Station

Grouting sections	Grouting pressure (MPa)	Theoretical diffusion radius (m)	Measured diffusion radius (m)
First section	0.6	2.833	2.2 to 2.5
Second section	0.8	3.012	2.5 to 2.8
Third section	1.5	4.175	3.5 to 4.0
Fourth, and Subsequent, sections	1.8	4.516	3.5 to 4.5

0.3 MPa, 0.6 MPa, 1.0 MPa, 0.6 MPa, 0.3 MPa. For each injection phase, the duration of water injection should be at least 20 minutes and should be stable at each designate value before moving on to the next loading phase. The grouting pressure and the lengths of corresponding sections were shown as follows: the first section comprising the bedrock was 2.0 m long and the grouting pressure was 0.6 MPa. The second and third sections were 3.0 m and 5.0 m long and needed grouting pressures of 0.8 MPa and 1.5 MPa, respectively. For the fourth and subsequent sections, the lengths were 5.0 m and the grouting pressures were 1.8 MPa. The diameter of the initial hole was 91 mm and the final hole diameter was no less than 59 mm. Table 3 shows the comparisons between the calculation results obtained by utilising the proposed model and measured values of slurry diffusion radius.

3.2.3 Comparisons between theoretically calculated and measured data

Based on analysis of Fig. 9, and Tables 3 and 4, the calculated results from the theoretical model in the above two engineering cases show consistent changes to those in the actual diffusion radius of the slurry, and the values of both are similar. Furthermore, the theoretically calculated value is much smaller than the results obtained by using the Lombardi formula and the Virko formula. The theoretical model of grouting established in this study can reflect slurry diffusion characteristics on the whole and the calculation results match engineering practice, so the results can play a guiding role in grouting operations.

Through further analysis, it is found that the theoretically calculated value of diffusion radius of slurry is slightly larger than the measured results in the field. The reasons for this are mainly as follows: (1) A lot of small cracks are found in the actual strata which have high water absorption but low groutability. Owing to the width of the crack in the theoretical model being determined through water pump-in testing, a large water absorption value leads to a large crack width, therefore, the theoretical value of slurry diffusion radius is large. (2) Grouting processes are complex, which influences the diffusion effects of slurry. For example, in the grouting process, after mixing a slurry, the blender keeps stirring for a long time, which leads to significant changes in the performance of the slurry. Moreover, slurry has a larger viscosity after entering the grouting hole and it solidifies in the grouting hole before diffusing. (3) In the grouting process, the sealing plug of the grouting hole needs to be replaced frequently, which interrupts grouting and results in deposition and solidification of slurry in the hole and seams, thus affecting the subsequent grouting effects; however, in the theoretical model, the stability of performance index of slurry is used, which fails to reveal the influences of the above factors. Therefore, the actual diffusion radius of slurry is smaller than the theoretically calculated value.

4. Influences of occurrence of cracks in rock masses on slurry diffusion characteristics

Based on the above theoretical model, the inclination angle α was set to 0°, 30°, 60°, and 90° and the azimuth angles of slurry diffusion were set to θ = 0°, 60°, 120°, and 180° herein. By substituting the calculation parameters in Table 1 into Eqs. (22) and (23), the relationships between grouting pressure under different occurrences of the oblique crack in rock masses with grouting time and slurry diffusion distance were studied.

4.1 Distribution characteristics of grouting pressure with time under different crack occurrences

Fig. 10 shows the changes in grouting pressure under different inclination angles and azimuth angles of slurry diffusion with time. As shown, with the increase of grouting time, the grouting pressure gradually increases. Grouting pressure grows slowly in the early stages of grouting, while it rises quickly in its later stages.

When the azimuth angle of slurry diffusion is $\theta \leq 90°$, that is, the direction of motion of the slurry is consistent with the inclination of the crack surface, as the inclination angle increases, the grouting pressure decreases within the same time. Because when the crack surface is inclined, a downward deadweight component acts on the slurry and overcomes slurry resistance together with the grouting pressure, promoting downward motion of the slurry. When grouting time, the azimuth angle of slurry diffusion, and inclination angle are t = 60, θ = 0°, and α = 90° separately, the grouting pressure of the oblique crack is 0.62 times that of a horizontal crack.

When the azimuth angle of slurry diffusion is $90° < \theta \leq 180°$, namely, the motion of slurry is opposite to the inclination of the crack surface, the larger the inclination angle, the greater the grouting pressure. The increased grouting pressure is used to overcome dual effects of deadweight and viscous resistance of the slurry. When the grouting time is 60 s, the grouting pressure of the oblique crack is 1.38 times that of horizontal crack under conditions where the azimuth angle of slurry diffusion is θ = 180° and the inclination angle is α = 90°.

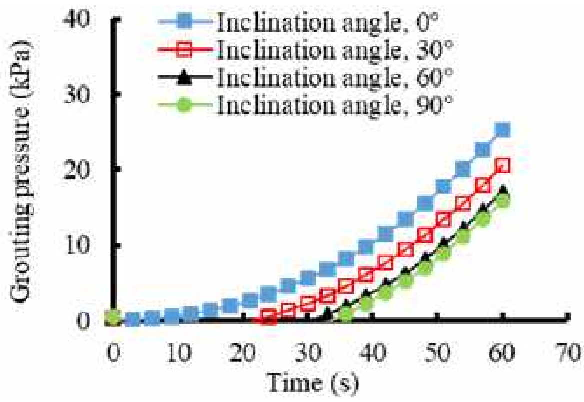

(a) Azimuth, 0°

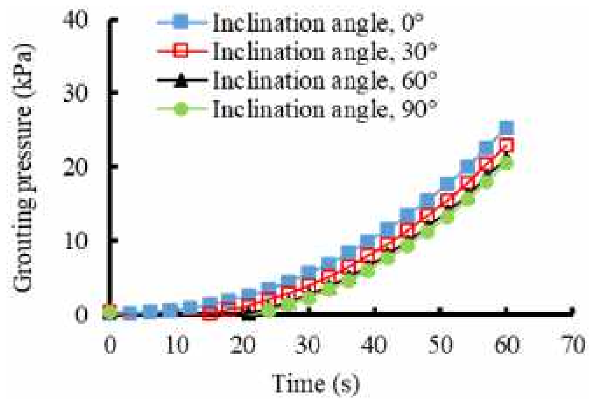

(b) Azimuth, 60°

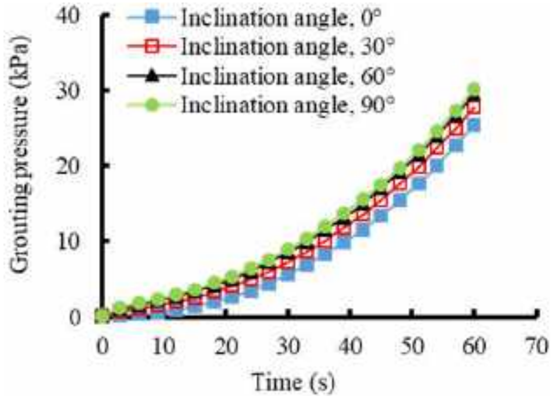

(c) Azimuth, 120°

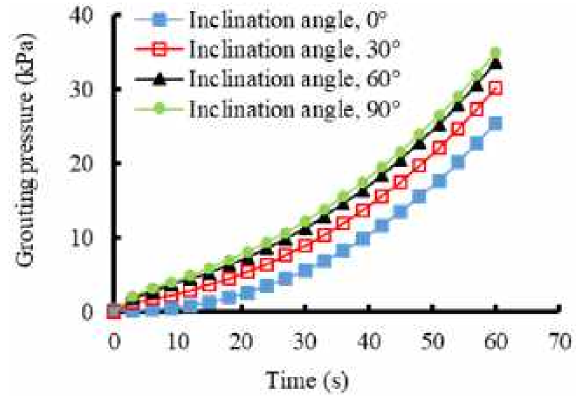

(d) Azimuth, 180°

Fig. 10 Curves of grouting pressure versus time under different crack occurrences in a rock mass

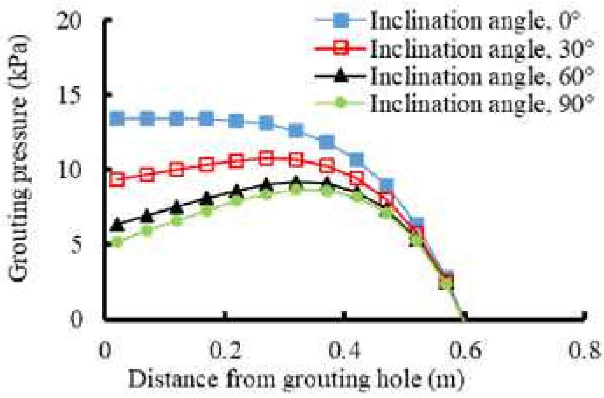

(a) Azimuth, 0°

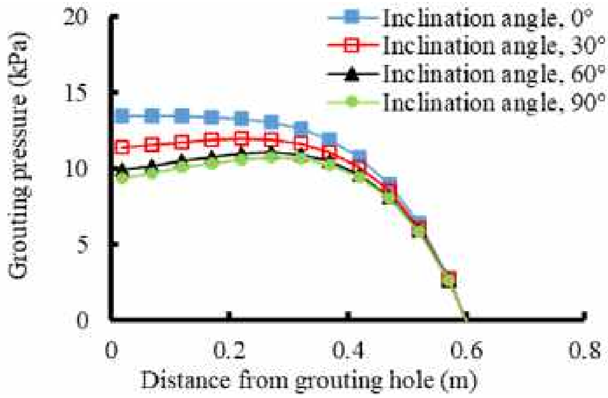

(b) Azimuth, 60°

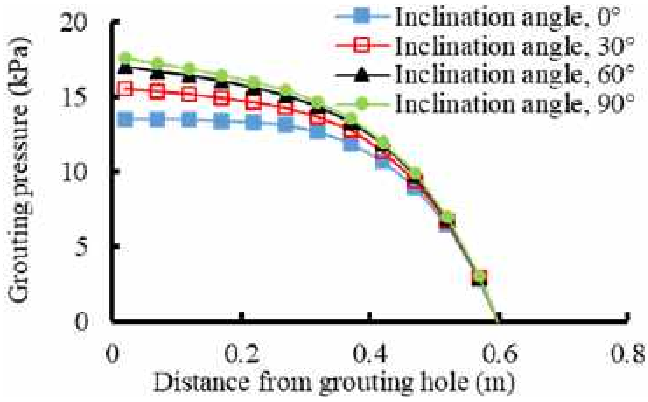

(c) Azimuth, 120°

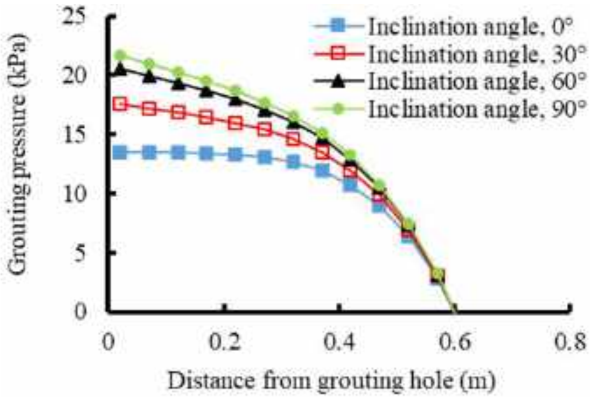

(d) Azimuth, 180°

Fig. 11 Curves of slurry pressure versus diffusion distance under different crack occurrences at t = 45 s

Crack occurrence in rock masses significantly affects the distribution characteristics of grouting pressure with time. Therefore, in the actual grouting process, the corresponding parameters of grouting pressure should be selected for grouting experiments by combining them with the spatial distribution characteristics of the cracks in such rock masses, thus improving grouting efficiency.

4.2 Spatial distribution characteristics of grouting pressure under different crack occurrences

Fig. 11 shows the relationship between grouting pressure and distance from the grouting hole under different inclination angles and azimuth angles of slurry diffusion when t = 45 s. With increasing distance from the grouting hole, the pressure in the slurry diffusion zone has obvious non-linear and non-uniform spatial characteristics.

When the azimuth angle of slurry diffusion is $\theta \leq 90°$, that is, the direction of motion of the slurry is consistent with the inclination of the crack surface, the grouting pressure first increases and then decreases with increasing distance from the grouting hole. The maximum grouting pressure appears at a certain position along the crack rather than in the surroundings to the grouting hole. The distance from the grouting hole mainly depends on azimuth angle of slurry diffusion in the crack and the deadweight and viscous resistance of the slurry. Furthermore, as the inclination angle increases, the pressures at positions located at the same distance from the grouting hole are smaller, because when the crack surface is inclined, a downward deadweight component acts on the slurry and overcomes the viscous resistance of the slurry together with the grouting pressure, promoting downward motion thereof. In the early stages of grouting, the grouting pressure in the oblique crack with an azimuth angle of slurry diffusion θ = 0° and inclination angle α = 90° near the grouting hole is 0.39 times that of the horizontal crack. In the later stages of grouting, grouting pressure fell rapidly, indicating that the viscosity of the slurry in the diffusion front is much higher than that near the grouting hole. Under these conditions, the influences of the deadweight of the slurry are small.

When azimuth angle of slurry diffusion is $90° < \theta \leq 180°$, that is, the direction of motion of the slurry is opposite that of the inclination of the crack surface, the grouting pressure attenuates from the grouting hole to the surrounding rock and the maximum grouting pressure is found near the grouting hole. In the early stages of grouting, the viscosity of the slurry is low and the pressure gradient around the grouting hole is small, so grouting pressure attenuates relatively slowly. With increasing inclination angle, the grouting pressure at that position located at the same distance from the center of the grouting hole increases accordingly. The reason for this is as follows: in an inclined crack, a downward deadweight component acts on the slurry, and the increased grouting pressure is used to overcome the dual effects of deadweight and viscous resistance of the slurry. In the rock surrounding the grouting hole in the early stages of grouting, the grouting pressure of the oblique crack with an azimuth angle of slurry diffusion θ = 180° and inclination angle α = 90° is 1.61 times that of the horizontal crack. In the later stages of grouting, the attenuation of grouting pressure shows obvious non-linear characteristics and the viscosity of slurry in the diffusion front is much higher than that near the grouting hole. At this time, the deadweight of slurry exerts little influence.

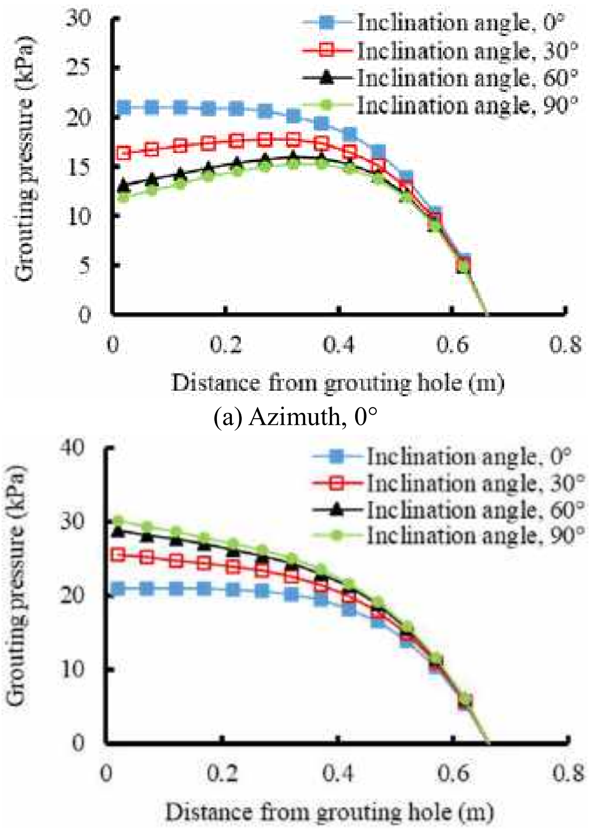

(a) Azimuth, 0°

(b) Azimuth, 180°

Fig. 12 Curves of slurry pressure versus diffusion distance under different crack occurrences at t = 5s5 s

By comparing Figs 11 and 12, the longer the grouting duration, the greater the grouting pressure at the position the same distance away from the center of the grouting hole, and the rate of changes increases significantly. This is mainly because the viscosity of slurry exhibits power function growth, which is consistent with the previous conclusions.

Crack occurrence in rock masses significantly affects spatial changes in grouting pressure. Therefore, the grouting pressure should be estimated according to grouting circles in different parts during engineering design and be adjusted constantly during construction.

5. Discussions

It is found from the above analysis that both the dipping angle of rock cracks and the diffusion direction angle of slurry have significant effects on the spatio-temporal variation of grouting pressure. This finding is consistent with the slurry diffusion characteristics observed in actual engineering, showing that the presented research is meaningful and valuable for engineering applications.

It should be noted that, for an actual slurry diffusion process, the material form of the quick-setting slurry often shows obvious phase transition characteristics in a short time. The phase transition refers to the transition from fluid to fluid plastic body, and finally to rigid body. The presented study, however, adopts a non-Newtonian fluid constitutive model so it cannot provide an accurate description of the complicated phase transition process. In this regard, it is promising to propose a constitutive model reflecting both the phase transition process and the mechanical properties of slurry. Moreover, the gelling time of quick-setting grouting materials is short, and the general duration is tens of seconds to several minutes. In such a short period of time, the later grouted slurry may cause splitting damage to the earlier gel-solidified slurry, thereby reducing the integrity of the calculus body and greatly affecting the grouting reinforcement effect for weak surrounding rock masses in field. This issue, regarding the rational quantitative analysis and evaluation, is another point that deserves further study.

6. Conclusions

(1) A theoretical model of slurry diffusion in an oblique crack in rock masses at constant grouting rate was presented by considering the deadweight of the slurry and the characteristics of the non-uniform spatial distribution of viscosity of fast-curing grouts. Furthermore, the relationship linking grouting pressure, grouting time, and slurry diffusion distance is quantified. Compared with the general grouting models established based on horizontal cracks, this model was not affected by crack occurrence, so it was could be used to find distribution characteristics of slurry diffusion in cracks of any spatial occurrence. The conclusions are generally applicable, which further extends the utility and ambit of this model.

(2) By using a 3-d finite element program in multi-field coupled software Comsol, we simulated the diffusion process of fast-curing grouts in the crack. Through the comparison of numerical simulation results and theoretical calculations, it is found that the trends in grouting pressure–time and grouting pressure–space curves obtained based on theoretical calculation and numerical simulation were consistent. The difference between them was small and the maximum discrepancy was no more than 10%, thus verifying the effectiveness of the proposed theoretical model. In addition, by analyzing the measured data recorded during grouting in two practical engineering case studies, and comparing the measured slurry diffusion range, with theoretically calculated values, it is found that they were similar. This indicated that the model could be applied to engineering practice and can provide guidance for grouting process design.

(3) Based on the research, crack occurrence in rock masses had significant impacts on the characteristics of slurry diffusion. When the azimuth angle of slurry diffusion is $\theta \leq 90°$, at the same time, the grouting pressure in the slurry diffusion zone first increased and then decreased with increasing distance from the grouting hole, while the grouting pressure and slurry pressure in the diffusion zone both decreased as the inclination angle increased. When $90° < \theta \leq 180°$, at the same time, the grouting pressure was attenuated with distance from the grouting hole, and the grouting pressure and slurry pressure in the diffusion zone both increased with inclination angle. Moreover, the increased grouting pressure overcame the dual effects of the deadweight and viscous resistance of the slurry. During grouting process, it is necessary to consider the spatial occurrence of cracks in rock masses.

Finally, it should be noted that, in the actual slurry diffusion process, physical forms of fast-curing grouts generally showed a phase transition within a short time. Namely, fluids were transformed into plastic bodies in a short time and were finally changed into rigid bodies. Therefore, it is difficult to describe such a complex phase transition process accurately by merely using a single constitutive model of a non-Newtonian fluid and it is necessary to examine the constitutive model further in future research. Moreover, the presented model is suitable for fractured rock mass containing joints where the slurry diffuses along fractures under grouting effect. For rock masses containing a large number of weak interlayers, the slurry may diffuse along the weak planes and cause bed rock rupture. Under these circumstances, the presented model should be improved to adapt to a more complicated situation. This topic will also be addressed in future research.

Acknowledgments

The work was supported by the National Science Foundation of China (Nos. 51539002, 51979008, 51779018, 51809014) and the Basic Research Fund for Central Research Institutes of Public Causes (Nos. CKSF2019434/YT, CKSF2019169/YT).

References

Anderson, J.D. and Wendt, J. (1995), *Computational Fluid Dynamics*, McGraw-Hill Education, New York, U.S.A.

Andjelkovic, V., Lazarevic, Z., Nedovic, V. and Stojanovic, Z. (2013), "Application of the pressure grouting in the hydraulic tunnels", *Tunn. Undergr. Sp. Tech.*, **37**, 165-179. http://doi.org/10.1016/j.tust.2012.08.012.

Bezuijen, A., Te Grotenhuis, R., Van Tol, A.F., Bosch, J.W. and Haasnoot, J.K. (2011), "Analytical model for fracture grouting in sand", *J. Geotech. Geoenviron. Eng.*, **137**(6), 611-620. https://doi.org/10.1061/(ASCE)GT.1943-5606.0000465.

Bouchelaghem, F. (2009), "Multi-scale modelling of the permeability evolution of fine sands during cement suspension grouting with filtration", *Comput. Geotech.*, **36**(6), 1058-1071. http://doi.org/10.1016/j.compgeo.2009.03.016.

Celik, F. (2019), "The observation of permeation grouting method as soil improvement technique with different grout flow models", *Geomech. Eng.*, **17**(4), 367-374. http://doi.org/10.12989/gae.2019.17.4.367.

Celik, F. and Canakci, H. (2015), "An investigation of rheological properties of cement-based grout mixed with rice husk ash (RHA)", *Constr. Build. Mater.*, **91**, 187-194. http://doi.org/10.1016/j.conbuildmat.2015.05.025.

Chen, T.L., Zhang, L.Y. and Zhang, D.L. (2014), "An FEM/VOF hybrid formulation for fracture grouting modelling", *Comput. Geotech.*, **58**, 14-27.

http://doi.org/10.12989/10.1016/j.compgeo.2014.02.002.
Cheng, H., Chen, J., Chen, R., Huang, J. and Li, J. (2019), "Three-dimensional analysis of tunnel face stability in spatially variable soils", *Comput*. *Geotech*., **111**, 76-88. http://doi.org/10.1016/j.compgeo.2019.03.005.
Dahlø, T.S. and Nilsen, B. (1994), "Stability and rock cover of hard rock subsea tunnels", *Tunn*. *Undergr*. *Sp*. *Tech*., **9**(2), 151-158. http://doi.org/10.1016/0886-7798(94)90026-4.
Devi, K., Saini, B. and Aggarwal, P. (2019), "Utilization of Kota stone slurry powder and accelerators in concrete", *Comput. Concrete*, **23** (3), 189-201. http://doi.org/10.12989/cac.2019.23.3.189.
Frank, M.W. (2015), *Fluid Mechanics*, McGraw-Hill Education, New York, U.S.A.
Fransson, Å., Tsang, C.F., Rutqvist, J. and Gustafson, G. (2007), "A new parameter to assess hydromechanical effects in single-hole hydraulic testing and grouting", *Int*. *J*. *Rock Mech*. *Min*. *Sci*., **44**(7), 1011-1021. http://doi.org/10.1016/j.ijrmms.2007.02.007.
Funehag, J. and Gustafson, G. (2008), "Design of grouting with silica sol in hard rock–New methods for calculation of penetration length, Part I", *Tunn*. *Undergr*. *Sp*. *Tech*., **23**(1), 1-8. http://doi.org/10.1016/j.tust.2006.12.005
GB175-2007 (2008), National Standard for Common Portland Cement, General Administration of Quality Supervision, Inspection and Quarantine of the People's Republic of China, Standards Press of China, Beijing, China.
Kim, J.S., Lee, I.M., Jang, J.H. and Choi, H. (2009), "Groutability of cement-based grout with consideration of viscosity and filtration phenomenon", *Int*. *J*. *Numer*. *Anal*. *Meth*. *Geomech*., **33**(16), 1771-1797. http://doi.org/10.1002/nag.785.
Lisa, H., Christian, B., Åsa, F., Gunnar, G. and Johan, F. (2012), "A hard rock tunnel case study: Characterization of the water-bearing fracture system for tunnel grouting", *Tunn*. *Undergr*. *Sp*. *Tech*., **30**, 132-144. http://doi.org/10.1016/j.tust.2012.02.014.
Lombardi, G. (1985), "The role of cohesion in cement grouting of rock", *Proceedings of the 15th International Congress of Large Dams*, Lausanne, Switzerland, June.
Miller, E.A. and Roycroft, G.A. (2004), "Compaction grouting test program for liquefaction control", *J*. *Geotech*. *Geoenviron*. *Eng*., **130**(4), 355-361. https://doi.org/10.1061/(ASCE)1090-0241(2004)130:4(355).
Mirza, J., Saleh, K., Langevin, M.A., Mirza, S., Bhutta, M.A.R. and Tahir, M.M. (2013), "Properties of microfine cement grouts at 4°C, 10°C and 20°C", *Constr*. *Build*. *Mater*., **47**, 1145-1153. http://doi.org /10.1016/j.conbuildmat.2013.05.026.
Ruan, W.J. (2005), "Spreading model of grouting in rock mass fissures based on time-dependent behavior of viscosity of cement-based grouts", *Chin*. *J*. *Rock Mech*. *Eng*., **24**(15), 2709-2714. https://doi.org/10.3321/j.issn:1000-6915.2005.15.018.
Seo, H.J., Choi, H. and Lee, I.M. (2016), "Numerical and experimental investigation of pillar reinforcement with pressurized grouting and pre-stress", *Tunn*. *Undergr*. *Sp*. *Tech*., **54**, 135-144. https://doi.org/10.1016/j.tust.2015.10.018.
Sha, F., Li, S., Liu, R., Li, Z. and Zhang, Q. (2018), "Experimental study on performance of cement-based grouts admixed with fly ash, bentonite, superplasticizer and water glass", *Constr*. *Build*. *Mater*, **161**, 282-291. https://doi.org/10.1016/j.conbuildmat.2017.11.034.
Te Grotenhuis, R. (2004), "Fracture grouting in theory: Modelling of fracture grouting in sand", Ph.D. Dissertation, Delft University of Technology, Delft, The Netherelands.
Wang, Y. and Su, B.Y. (2002), "Research on the behavior of fluid flow in a single fracture and its equivalent hydraulic aperture", *Adv*. *Water Sci*., **13**(1), 61-68. https://doi.org/10.1002/mop.10502.
Wittke, W. (1991), "The application of grouting with dense cement paste", *Proceedings of the Collection of Translations of Modern Grouting Techniques*. Beijing, China, January.
Yoon, J. and El Mohtar, C.S. (2015), "A filtration model for evaluating maximum penetration distance of bentonite grout through granular soils", *Comput*. *Geotech*., **65**, 291-301. https://doi.org/10.1016/j.compgeo.2015.01.004.
Zhang, Q.S., Zhang, L.Z., Liu, R.T., Li, S.C. and Zhang, Q.Q. (2017), "Grouting mechanism of quick setting slurry in rock fissure with consideration of viscosity variation with space", *Tunn*. *Undergr*. *Sp*. *Tech*., **70**, 262-273. https://doi.org/10.1016/j.tust.2017.08.016.
Zhang, Q.S., Zhang, L.Z., Zhang, X, Liu, R.T., Zhu, M.X. and Zheng, D.Z. (2015), "Grouting diffusion in a horizontal crack considering temporal and spatial variation of viscosity", *Chin*. *J*. *Rock Mech*. *Eng*., **34**(6), 122-134. https://doi.org/10.13722/j.cnki.jrme.2014.0958.
Zhong, D.H., Yan, F.G., Li, M.C., Huang, C.X., Fan, K. and Tang, J.F. (2015), "A real-time analysis and feedback system for quality control of dam foundation grouting engineering", *Rock Mech*. *Rock Eng*., **48**(5), 1947-1968. https://doi.org/10.1007/s00603-014-0686-6.
Zhou, F., Sun, W., Shao, J., Kong, L. and Geng, X. (2020), "Experimental study on nano silica modified cement base grouting reinforcement materials", *Geomech*. *Eng*., **20**(1), 67-73. https://doi.org/10.12989/gae.2020.20.1.067.
Zhou, Y., Wang, G.H. and Chang, Y.H. (2019), "Comparison of the effect of lithium bentonite and sodium bentonite on the engineering properties of bentonite-cement-sodium silicate grout", *Adv*. *Concrete Construct*., **9**(3), 279-287. https://doi.org/10.12989/acc.2020.9.3.279.

CC